92-219

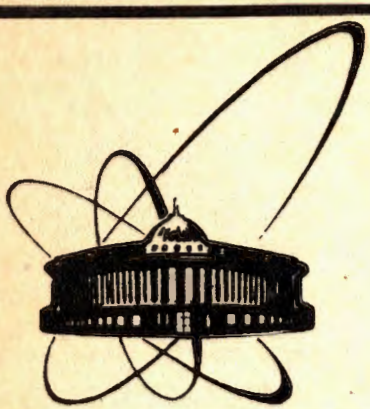

объединенный
институт
ядерных
исследований
дубна

E13-92-219

Ju.A.Budagov, G.A.Chlachidze[1], I.P.Liba, S.N.Malyukov,
I.A.Minashvili[1], N.A.Russakovich, N.L.Russakovich,
G.V.Velev[2]

STUDY OF A 260-CHANNEL LEAD GLASS CALORIMETER

Submitted to "NIM"

[1]High Energy Physics Institute of the Tbilisi State University, Tbilisi, Georgia
[2]Computer Center of Physics, Bulgarian Academy of Sciences, Sofia, Bulgaria

1992

1. Introduction

Lead glass Cherenkov counter arrays have been widely used for electromagnetic shower calorimeters [1-6]. They have a good energy resolution for the detection of high energy electrons (positrons) and photons [7-8].

In this paper an electromagnetic calorimeter of lead glass type, comprising 260 counters, is investigated. The detector has been used in the HYPERON [9-11] spectrometer for registration of the neutral products from decays of K^* mesons. The setup has been installed in a 3-15 GeV positively charged beam extracted from the IHEP accelerator.

We report here an energy and spatial resolution of the calorimeter. Its parameters are used at the kinematic fitting for K^* decays identification.

2. Geometry

The 260-channel lead glass shower hodoscope detector (SHD-260) is a matrix of 19x15 cells with a hole of 5x5 cells in the center (fig. 1) and its surface is perpendicular to the beam axis. For test measurement we used a part of 5x5 counters (fig. 1, bottom).

In our experiments the SHD-260 detects gamma quanta and positrons with energy 0.5-5 GeV and an angular region from 2.5^0 to 16^0 with respect to the beam axis.

3. Electromagnetic calorimeter

The sketch of one SHD-260 module is shown in fig. 2. The counter is made of TF1-000 lead glass with dimensions 10x10 cm^2 and length 35 cm (14 radiation lengths).

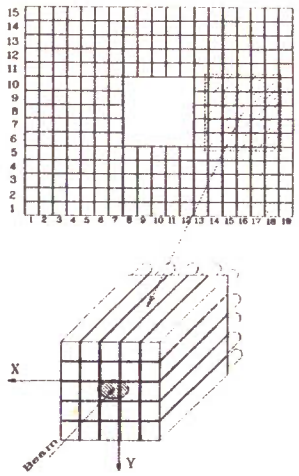

Fig. 1 Front view of SHD-260: the whole detector and the test part of 5x5 counters (bottom).

The Cherenkov light is registered with a photomultiplier FEU-110 (diameter of the photocathode is 68 mm) which is glued to one of the sides of the lead glass. For improvement of the light collection the lead glass surfaces were polished and wrapped up in aluminized mylar. The glass block was placed in a tin housing with a thickness 0.6 mm. The FEU-110 was also put into a steel frame and wrapped up in a permalloy magnetic screen.

For on-line control of the stability of the spectrometer channels light-emitting diodes (LED) as light pulse sources are used. The light pulses are transmitted from LEDs to the counters by optic fibers (fig. 2).

The SHD-260 is placed on a platform which gives a possibility of moving the detector vertically and horizontally across the beam. Thus each counter can be positioned on the beam line with 1.5 mm accuracy during the spectrometer calibration.

The SHD-260 module and the whole detector are described in more detail in ref. [10].

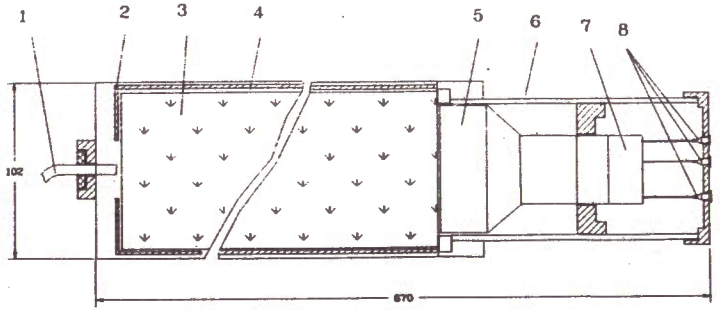

Fig. 2 A module of the calorimeter SHD-260: (1) optic fiber to distribute light pulses of the monitoring system; (2) tin housing (0.6 mm thick); (3) TF1-000 lead glass radiator; (4) permalloy magnetic screen; (5) photomultiplier FEU-110; (6) steel frame; (7) high voltage divider; (8) high voltage and high frequency connectors.

3

4. Experimental procedure

The SHD-260 has been tested in the 18 channel beam at the IHEP U-70 accelerator.

Positrons were selected with the help of four threshold Cherenkov counters. The beam coordinates were defined by two blocks of proportional chambers with a 2 mm pitch. There were 10 planes of chambers placed in each projection. The positron impact point was determined with an error less than 1.0 mm.

The beam momentum was varied from 3 to 8 GeV/c and the beam momentum resolution was better than 2%.

Each of the SHD-260 counters (fig. 1) was centered perpendicularly to the beam direction and a sample of about 500 shower data were collected to calibrate the energy response.

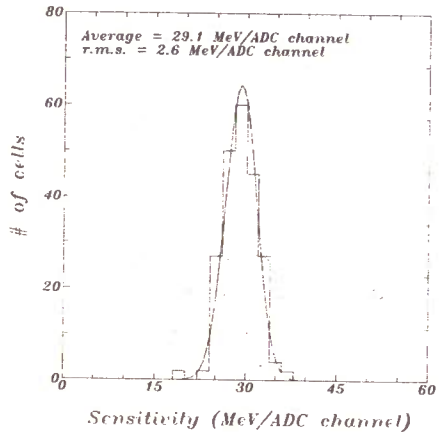

Fig. 3 Counter sensitivity.

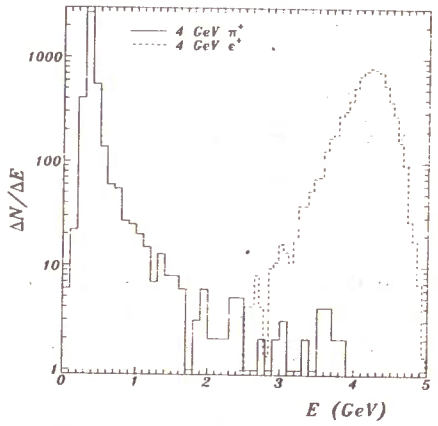

Fig. 4 Counter response from 4 GeV π^+ mesons and positrons.

5. Results.

5.1 Energy calibration and linearity

The calibration coefficient distribution for the whole detector is shown in fig. 3. The mean value (≈30 MeV/ADC-channel) is defined by the range of the measured positron and photon energy in our experiments and by the properties of the ADC (8-bit charge-sensitive analog-to-digital converters type KA008 [12,13] made to CAMAC standard).

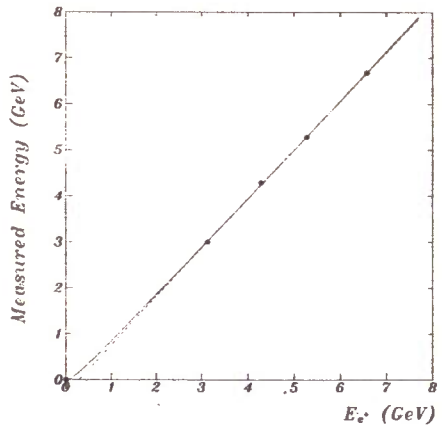

Fig. 5 Linearity of the energy response of the spectrometer.

A lead glass counter response from 4 GeV π^+ mesons obtained for the case of positron calibration is shown in fig. 4 with the response to positrons of the same energy superimposed. The number of the events under the peaks is equal. With a cut, which accepts 98% of the positrons (about 2.5 GeV), the pion contamination could be suppressed to 0.4%

Fig. 5 shows the measured energy as a function of the positron beam energy. A deviation from linearity is observed to the region below 3 GeV. We suppose that this effect is connected with attenuations of the Cherenkov light in the lead glass blocks which depends on the distance between the photocathode and the maximum of the shower development.

5.2 Losses of the electromagnetic shower in the gaps between the cells

In this SHD-260 module design we have around 0.5% of the nonactive volume. This small percentage practically guarantees that positrons and gamma quanta cannot be missed due to only passing through passive material. However, some fraction of the electromagnetic shower is lost in the gaps having a full thickness ≈ 1.2 mm (the walls of tin housings, the permalloy magnetic screens and the air layer) between adjacent lead glass blocks. The effect of this leakage depends on the impact point of the beam. The ratio of the energy response E_{res} to the beam energy E_{beam} as a function of the coordinate x of the impact position is shown in fig. 6. This result was obtained for the positron energies 3, 5 and 7 GeV. Fig. 6 shows that the signal loss is maximal (≈ 25%) when the shower axis is near to the gap, while it is small in the center of the counter.

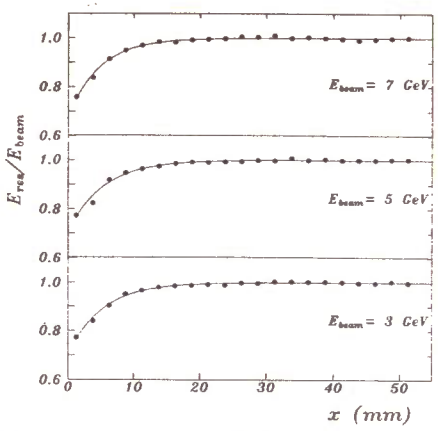

Fig. 6 Ratio of the energy response to the full beam energy.

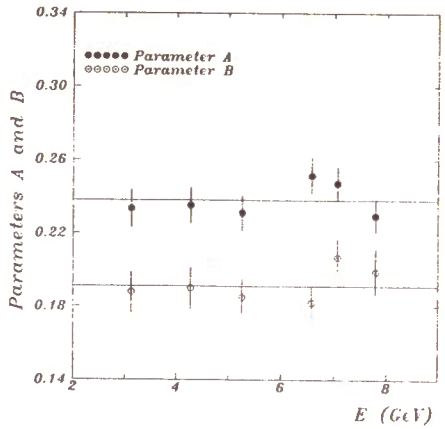

Fig. 7 Parameters A and B in the function (1) for the energy correction.

We parametrized this ratio with the expression

$$E_{res}/E_{beam} = 1 - A \exp(-Bx). \qquad (1)$$

The result from the fit is shown in fig. 6 (full line). In the two-dimensional case, the ratio E_{res}/E_{beam} should be

$$E_{res}/E_{beam} = 1 - A \exp(-Bx) - A \exp(-By),$$

where x and y are the coordinates of the beam impact position.

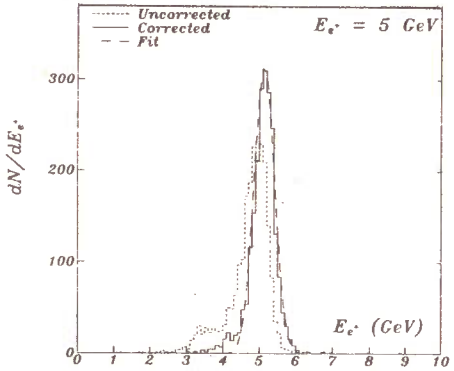

Fig. 8 Energy distribution obtained by sending the beam near the gaps; dashed line: uncorrected, full line: after correction.

Fig. 7 shows parameters A and B as a function of the positron energy. It is seen that the parameters A and B are almost independent of the positron energy in the interval 3-8 GeV. The weighted averages are A = 0.238±0.014 an B = 0.191±0.013 (the full lines, fig. 7).

Fig. 8 shows the measured energy distribution obtained by sending the 5 GeV/c beam near the gaps in the block

corners (dashed line) and the corrected energy distribution (full line). After correction the energy resolution is improved (σ_E/E = 7.5%) and the mean of the peak coincides with the average value of the positron energy.

5.3 Energy resolution

The energy resolution for one cell is mainly determined by the shower fluctuations and the photoelectron statistics.

The measured r.m.s. energy resolution is shown in fig. 9. The experimental data were collected for positron energies from 3 to 8 GeV when the beam impact point was in a 2x2 cm^2 square in the center of the cell. Thus the largest part of the electromagnetic shower was developed only in one counter and the amplitudes in the adjacent counters were equal to zero. We made a fit with two functions

$$\frac{\sigma_E}{E} = a + \frac{b}{\sqrt{E\ [GeV]}} \qquad (2)$$

and

$$\frac{\sigma_E}{E} = a \oplus \frac{b}{\sqrt{E\ [GeV]}} \qquad (3)$$

where E is the energy of the positrons and the symbol ⊕ means a quadratic sum.

In the first case (function (2)), the best fit gives (the full line, fig. 9)

$$a = (1.0 \pm 0.2)\times 10^{-2},$$

$$b = (6.0 \pm 0.6)\times 10^{-2}\ \ GeV^{1/2}.$$

In the second case we used for fitting the function (3) (the dashed line, fig. 9) and obtained

$$a = (2.0 \pm 0.2)\times 10^{-2},$$

$$b = (7.1 \pm 0.5)\times 10^{-2}\ \ GeV^{1/2}.$$

We also investigated the energy resolution when the shower was developed into 2 and 4 cells (fig. 10). The fit was done with two functions similar to (2) and (3), adding quadratically third

contribution

$$\frac{\sigma_E}{E} = a + \frac{b}{\sqrt{E\ [GeV]}} \oplus \frac{c_n}{\sqrt{E\ [GeV]}} \qquad (4)$$

and

$$\frac{\sigma_E}{E} = a \oplus \frac{b}{\sqrt{E\ [GeV]}} \oplus \frac{c_n}{\sqrt{E\ [GeV]}} \qquad (5)$$

where n is the number of the counters contributing to the energy reconstruction (n=2,4). The best fits for the both function (4) and (5) give in the limit of statistical accuracy the same results for parameters c_2 and c_4

$$c_2 = (7.2 \pm 0.5)\times10^{-2} \quad GeV^{1/2}$$

$$c_4 = (8.8 \pm 0.6)\times10^{-2} \quad GeV^{1/2}.$$

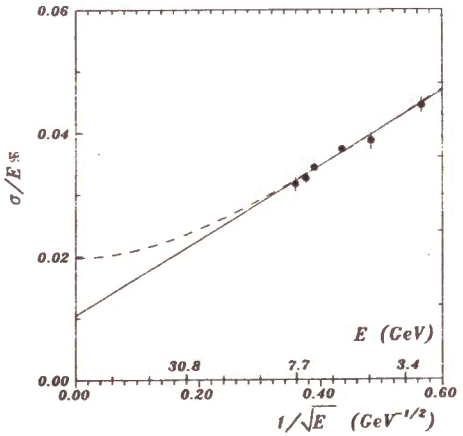

Fig. 9 Energy resolution for one cell. The full line is the result of the fit with form (2). The dashed line is a fit with (3).

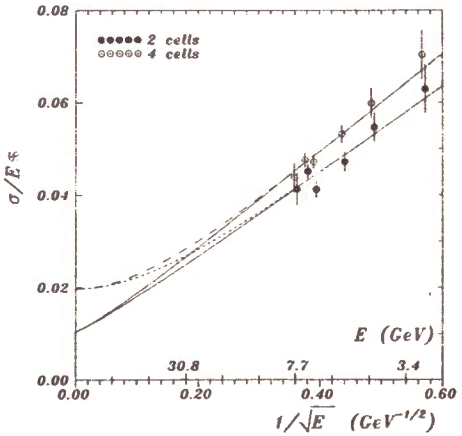

Fig. 10 Energy resolution for two and four cells. The full lines are fits with form (4) and the dashed lines are the results of the fits with form (5).

We suppose that the reason for the arising of the third term is the inaccuracy in the energy determination as a consequence of the energy losses in the passive materials in the gaps between the lead glass blocks.

5.4 Determination of the shower position and a spatial resolution

We obtained a function for the determination of the shower position (coordinate function) using the results of the simulation based on the GEANT 3 [14] program. Electromagnetic showers from positrons with energies from 0.3 to 8 GeV were generated in the lead glass media.

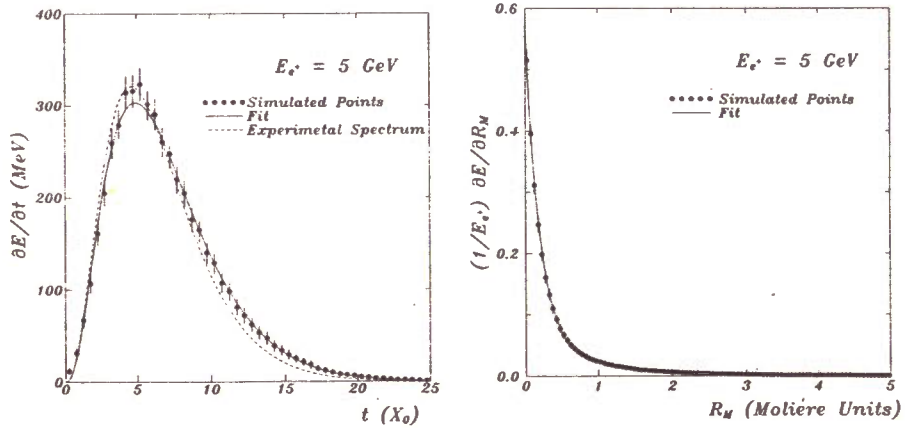

Fig. 11 Characteristics of the showers from 5 GeV positrons: (a) the longitudinal development; full line: the result of simulation, dashed line: experimental distribution from ref. [15]; (b) simulated distribution of the transverse development of the shower.

Fig. 11a,b show the longitudinal and transverse development of the shower produced by 5 GeV positrons (full line) as a result of the Monte-Carlo simulation. In fig. 11a there is also an experimental distribution of the longitudinal development of the 5 GeV electromagnetic positron showers from ref. [15] (dashed line). The experimental data from ref. [15] were obtained in the same medium by registration of Cherenkov light. The good agreement between the experimental spectrum and the simulated data (fig. 11a) obtained without accounting for the Cherenkov light collection enables us to be confident about our simulated results and their use for the determination of the detector parameters.

We parametrized the transverse energy distribution at the lead glass depth of 14 radiation lengths (fig. 11b) with the sum

of two exponents [7,16]

$$\frac{1}{E_{e^+}}\frac{\partial E}{\partial r} = C_1 \exp(-r/\lambda_1) + C_2 \exp(-r/\lambda_2) \quad (6)$$

where r is the distance from the shower axis in the Molière units, λ_1 and λ_2 are the attenuation lengths for the central and peripheral parts of the electromagnetic shower.

In the region from 0.5 to 8 Gev the parameters C_1, C_2, λ_1 and λ_2 do not depend on the positron energy. The fits of transverse distributions are obtained with $C_1 = 0.512$, $C_2 = 0.0543$, $\lambda_1 = 0.202$ and $\lambda_2 = 1.03$ (the errors are $\approx 0.2\%$).

We numerically integrated the form (6) in the bounds $y \in [-6.0\ R_M, 6.0\ R_M]$ $x \in [-6.0\ R_M, x_b]$ (R_M is the Molière radius). Thus we obtained the ratio E_{x_b}/E_{e^+} as a function of x_b and parametrized (fig. 12) with the expression

$$\frac{E_{x_b}}{E_{e^+}} = a_1 \arctan(a_2 + a_3 (x_s - x_b)) \quad (7)$$

where x_s is the coordinate of the shower axis.

The fits of the experimental (dashed curve, fig. 12) and simulated (full curve, fig. 12) data give no significant difference within statistical accuracy for the parameters a_1-a_3.

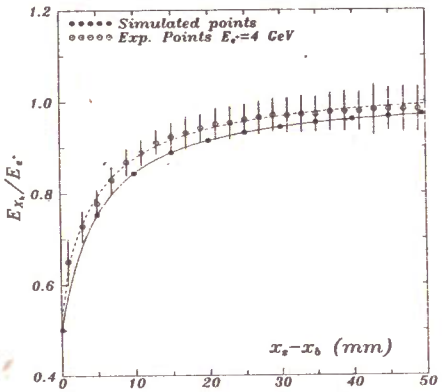

Fig. 12 The ratio E_{x_b}/E_{e^+} for 5 GeV positrons; full line: fit of simulation points, dashed line: fit of experimental data. The result of the fits is described in the text.

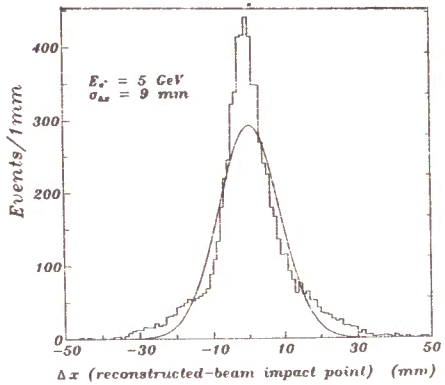

Fig. 13 Distribution of the difference Δ x between the positron coordinate reconstructed by the calorimeter and the one given by the proportional chambers. The curve is a fit to the data with a Gaussian function.

The result from fitting of the simulated points is

$$a_1 = 0.647 \pm 0.001$$
$$a_2 = 0.997 \pm 0.003$$
$$a_3 = 0.26 \pm 0.02 \quad mm^{-1}.$$

Using expression (7) we obtained an one-dimensional coordinate function in the following form

$$x_s = \frac{1}{a_3}\left(\tan\frac{R}{a_1} - a_2\right) \quad mm \quad (8)$$

where R is E_{x_b}/E_{e^+} at $x_b = 0$ (similar functions were used in ref. [17,18]).

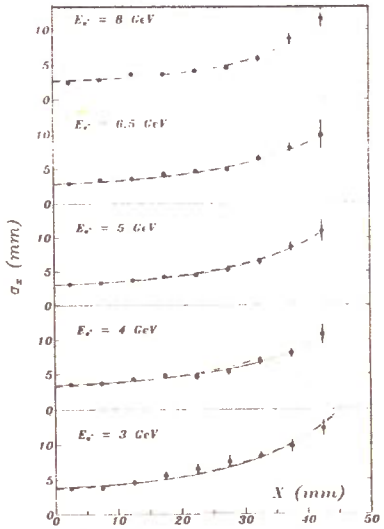

Fig. 14 The spatial resolution as a function of the beam position and the positron energy; full line: independent fits, dashed line: simultaneous fit of the spatial resolution data.

The global distribution of the difference between the beam impact point and the reconstructed coordinate with (8) is shown in fig. 13. The full curve is a parametrization with a Gaussian function (σ_x = 9 mm). It can be seen that the distribution has not a Gaussian form. This histogram is really a sum of normal distributions with different r.m.s. It arises from the dependence of the spatial resolution on the beam impact position.

We have also studied the dependence of the spatial resolution on the beam impact position (fig. 14). The full curve is the fit with an exponent

$$\sigma_x = c_3 (1 + c_1 \exp(c_2 x) \quad mm.$$

The parameters c_1 and c_2 do not depend on the positron energy. The parameter c_3 was parametrized with

$$c_3 = b_1 + \frac{b_2}{\sqrt{E\ [GeV]}}$$

From the simultaneous fitting of the experimental data for

3-8 GeV with the expression

$$\sigma_x = (b_1 + \frac{b_2}{\sqrt{E\ [GeV]}})\ (1 + c_1 \exp(c_2\ x) \quad mm$$

(the dashed curve, fig. 14) we obtained the following parameter values

$$c_1 = 0.23 \pm 0.04$$
$$c_2 = 0.062 \pm 0.006\ mm^{-1}$$
$$b_1 = 0.64 \pm 0.05\ mm$$
$$b_2 = 4.12 \pm 0.37\ GeV^{1/2}.$$

The confidence level of this fit is 73%.

Thus we parametrized the spatial resolution of SHD-260 as a two-dimensional function of the positron energy and the coordinate of the beam impact point.

5.5 Reconstruction of π^0 and η mesons

A test of the global characteristics of the SHD-260 is the reconstruction of the gamma-gamma invariant mass.

We used a decay $K^+ \longrightarrow \pi^+\pi^0$ to produce π^0's and 10 GeV π^+ beams hitting a deuterium target 27.5 cm thick to produce η mesons

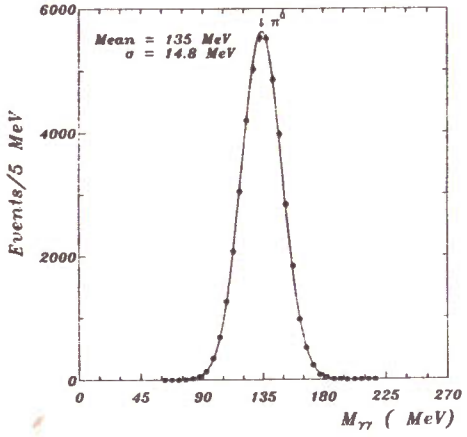

Fig. 15 γ-γ mass spectrum for showers from the decay $\pi^0 \longrightarrow 2\gamma$.

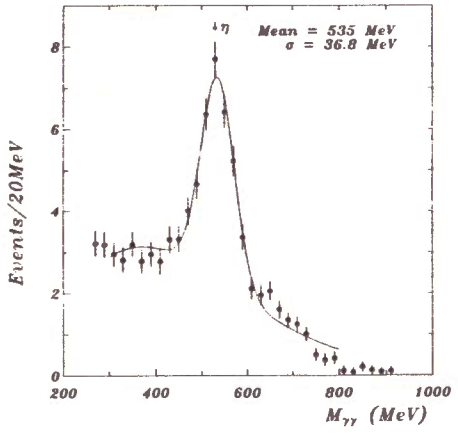

Fig. 16. γ-γ invariant mass in the η mass region.

in the reaction [19]

$$\pi^+ + D \longrightarrow \eta + X.$$
$$\hookrightarrow 2\ \gamma$$

The gamma-gamma invariant mass (M) for showers with reconstructed energy $E_\gamma > 0.7$ GeV from $K^+ \longrightarrow \pi^+\pi^0$ decays is shown in fig. 15. The π^0 peak has a width of 30 MeV (FWHM) and $\sigma_M/M \approx 11\%$. The background outside the peak is very small (< 0.5%).

The typical spectrum for the gamma-gamma invariant mass in the η mass region is shown in fig. 16. The spread of the peak is $\sigma_M/M = 7\%$.

These results correspond to the resolution expected from the coordinate and energy accuracy of the SHD-260 and are comparable with the resolution of other lead glass detectors with smaller dimensions of the cells [2,3,6].

6. Conclusion

We have determined the characteristics of a 260-channel Cherenkov hodoscope calorimeter made of lead glass blocks with dimensions 10x10x35 cm^3. It has been tested in a 3-8 GeV/c positron beam.

The energy resolution of the calorimeter was obtained when the shower was developed in one, two and four counters. The spatial resolution was parametrized as a two dimensional function of the beam energy and coordinate of impact position.

The calorimeter has been used in experiments investigating K^+ meson decays and reactions of an η meson production. The obtained gamma-gamma invariant mass resolution is comparable with the resolution of other similar detectors.

Acknowledgements

We would like to thank V.N. Kolosov and V.I. Romanovscky of IHEP Protvino for the useful remarks and for the discussion of the results.

We are grateful to Professor V.B. Flyagin for the helpful attention to the work.

References

[1] D.P. Barber et al. Nucl. Instr. and Meth. 145 (1977) 453.

[2] F. Binon et al. Nucl. Instr. and Meth. 188 (1981) 507.
F. Binon et al. Nucl. Instr. and Meth. A248 (1986) 86.

[3] P. Checchia et al. Nucl. Instr. and Meth. A248 (1986) 317.
P. Checchia et al. Nucl. Instr. and Meth. A275 (1989) 49.

[4] S. Kawabata et al. Nucl. Instr. and Meth. A270 (1989) 50.

[5] T. Sumiyoshi et al. Nucl. Instr. and Meth. A271 (1988) 432.

[6] G.T. Bartha et al. Nucl. Instr. and Meth. A275 (1989) 59.

[7] S. Ivata, DPNU-3-79, Nagoya University, Japan (1979).

[8] Yu.D. Prokoshkin, Proc. of the 2-nd ICFA Workshop on Possibilities and Limitations of Accelerators and Detectors, Les Diablerets, Switzerland, ed. U. Amaldi (CERN, Geneva, 1979) p. 347.

[9] V.A. Antyukhov et al. Prib. Tekh. Eksp. 5 (1985) 35.

[10] G.S. Bitsadze et al. Prib. Tekh. Eksp. 4 (1987) 52.

[11] S.A. Akimenko et al. Prib. Tekh. Eksp. 1 (1988) 45.

[12] V.A. Antyukhov et al. JINR 10-12912, Dubna, 1979.

[13] V.A. Antyukhov et al. JINR 10-83-900, Dubna, 1979.

[14] R. Brun et al. GEANT 3, CERN DD/EE/84-1, 1987.

[15] G.S. Bitsadze et al. JINR E1-86-87, Dubna, 1986.

[16] G.A. Akopdjanov et al. Nucl. Instr. and Meth. 140 (1977) 441.

[17] S.A. Akimenko et al. IHEP 84-194, Serpukhov, 1984.

[18] G.S. Bitsadze et al. Nucl. Instr. and Meth. A311 (1992) 472.

[19] G.S. Bitsadze et al. Nucl. Phys. B279 (1987) 770.
Yu.A. Budagov et al. JINR E1-91-496, Dubna, 1991.

Received by Publishing Department
on May 25, 1992.

Будагов Ю.А. и др.
E13-92-219

Изучение 260-канального калориметра
из свинцового стекла

Изучены характеристики 260-канального черенковского годоскопического калориметра из свинцового стекла при облучении пучком позитронов с энергиями от 3 до 8 ГэВ. Определена зависимость энергетического разрешения от количества элементов калориметра, участвующих в восстановлении электромагнитного ливня. Пространственное разрешение детектора получено как функция энергии и координаты попадания позитронов.

Работа выполнена в Лаборатории ядерных проблем ОИЯИ.

Препринт Объединенного института ядерных исследований. Дубна 1992

Budagov Ju.A. et al.
E13-92-219

Study of a 260-Channel Lead Glass Calorimeter

The characteristics of a 260-channel Cherenkov hodoscope calorimeter made of lead glass blocks have been studied in a 3-8 GeV positron beam. The energy resolution was obtained in dependence on the number of the counters contributing to the reconstruction of the electromagnetic shower. The spatial resolution was parametrized as a function of the positron energy and the beam impact position.

The investigation has been performed at the Laboratory of Nuclear Problems, JINR.

Preprint of the Joint Institute for Nuclear Research. Dubna 1992